Anisotropic vortex core in the nematic state in electron-doped iron-pnictide superconductors

Hong-Yi Chen
Department of Physics, National Taiwan Normal University, Taipei, 116, Taiwan
(Revised 25 December 2023)

Based on a phenomenological model with competing nematic order and extended s-wave superconductivity, the vortex states in the electron-doped $BaFe_{1.8}Co_{0.2}As_2$ are investigated by solving Bogoliubov–de Gennes' equations. The spin-driven nematic order is considered for the optimally doped compound. Our results show that there is no Andreev bound states at the Fermi energy in the nematic phase. The double-peak structure of the local density of states is favorable to scanning tunneling microscopy experiments. We also propose an oval shape of the vortex structure in the local density of states map which is attributed to the existence of the nematic order.

PACS numbers: 74.25.Jb, 74.25.Ha, 74.20.Mn

I. INTRODUCTION

Iron-pnictide superconductors have compelling evidence for the observed nematicity in an exotic phase between the striped spin-density-wave (SDW) and superconducting (SC) order. The relation between the superconductivity and nematicity has become one of the essential issues in Fe-based superconductors. In this regard, investigating the vortex core states can provide useful information on the interplay between the nematicity and SC, as well as the SDW.

Recently, the scanning tunneling microscopy (STM) measurement on hole-doped $Ba_{1-x}K_xFe_2As_2$ samples has reported the existence of a clear Andreev bound states at the vortex core. The local density of states (LDOS) is asymmetrically peaked at the energy below the Fermi energy [1]. On the other hand, there are no bound states been reported on electron-doped $BaFe_{1.8}Co_{0.2}As_2$ samples [2]. The LDOS does not show any subgap peaks at the vortex core.

Theoretically, many authors have successfully demonstrated the existence of bound states at the vortex core in the hole-doped regime based on a two-orbital model [3-5]. The calculated LDOS shows an asymmetric peak at the energy below the Fermi energy. Meanwhile, several authors also use the two-orbital model and predict a peak at the energy above the Fermi energy in the electron-doped regime [6-9]. However, the theoretical predictions on the electron-doped samples have contrasted with the experimental results. Therefore, it is an important issue to develop a theory for the vortex core states in iron-pnictide superconductors.

Lately, the nematic phase has been reported in many experiments in electron-doped samples. The nematic order is possibly driven by electron spins and characterized by the spontaneous breaking of the tetragonal symmetry [10-24]. As a result, the spin-driven nematic order does not develop any SDW gap due to the antiferromagnetism along the x- and y-directions [25,26]. However, in the presence of a magnetic field, the magnetization might be locally enhanced in the vortex core as the nematic order exists ubiquitously. The induced magnetic moment would cause a local gap at the Fermi energy in the LDOS and split the conductance peak into two peaks. Such a double-peak structure can account for the non-observation of the subgap peaks in the optimally doped region of electron-doped samples. Therefore, the existence of the nematic order is a good candidate to explain the vortex structure in iron-pnictide superconductors.

In this paper, we study vortex core states with the interplay between SC and nematicity by a two-orbital Hamiltonian on a two-dimensional lattice. The spin-driven nematic order is incorporated as two modulated stripes of magnetizations inter-penetrate each other which has reported in our previous work [26]. The LDOS is performed to be compared with STM experiments. We show that the disappearing of the resonance peak in the LDOS is in qualitative agreement with STM experiments. Moreover, the effect of nematic order on vortex core structure is also discussed. The integrated spectrum of LDOS maps exhibits an oval shape of the vortex core, which we predict to be measurable by future experiments.

The rest of paper is organized as follows. In Sec. II, we develop a mean-field two-orbital Hamiltonian on a square lattice and apply a magnetic field. In sec. III, we performed the numerical calculation of Bogoliubov-de Gennes (BdG) equations. In sec. IV, we calculate the LDOS at the vortex core center, at the site outside the vortex core, and present the integrated spectrum of

LDOS maps. Finally, sec. V gives conclusions of the results.

II. MODEL AND FORMALISM

We begin with a two-orbital model on a two-dimensional lattice and consider the on-site interaction which is solely responsible for the magnetization and the next-nearest-neighbor attraction which causes the s^{+-} pairing [26]. The effective mean-field Hamiltonian can be written as,

$$\widehat{H} = \widehat{H}_0 + \widehat{H}_\Delta + \widehat{H}_{\text{int}} \quad (1)$$

$$\widehat{H}_0 = \sum_{ijuv\sigma} t_{ijuv}\, \hat{c}^\dagger_{iu\sigma} c_{jv\sigma} - \mu \sum_{iu\sigma} \hat{n}_{iu\sigma}$$

$$\widehat{H}_\Delta = \sum_{iju\sigma} \left(\Delta_{iju} \hat{c}^\dagger_{iu\sigma} \hat{c}_{ju\sigma'} + \text{H.c.}\right)$$

$$\widehat{H}_{\text{int}} = U \sum_{\substack{iu \\ \sigma\neq\sigma'}} \langle \hat{n}_{iu\sigma'}\rangle \hat{n}_{iu\sigma} + U' \sum_{\substack{i,u<v \\ \sigma\neq\sigma'}} \langle \hat{n}_{iu\sigma'}\rangle \hat{n}_{iv\sigma} + (U' - J_H) \sum_{i,u<v,\sigma} \langle \hat{n}_{iu\sigma}\rangle \hat{n}_{iv\sigma}$$

Here, i, j are the site indices, $u, v = 1, 2$ are the orbital indices, σ represents the spin, μ is the chemical potential, and $\langle n_{iu\sigma}\rangle$ is the electron density. The hopping matrix elements t_{ijuv} are chosen as [26, 27]

$$t_{i,i\pm x(y),u,u} = t_1 = -1.0,$$
$$\begin{cases} t_{i,i\pm(x+y),u,u} = \frac{1+(-1)^{x+y+u}}{2} t_2 + \frac{1-(-1)^{x+y+u}}{2} t_3 = 0.08, \\ t_{i,i\pm(x-y),u,u} = \frac{1+(-1)^{x-y+u}}{2} t_3 + \frac{1-(-1)^{x-y+u}}{2} t_2 = 1.35, \end{cases}$$
$$t_{i,i\pm(x\pm y),u,v\neq u} = t_4 = -0.12,$$
$$t_{i,i\pm x(y),u,v\neq u} = t_5 = 0.09,$$
$$t_{i,i\pm 2x(2y),u,u} = t_6 = 0.25,$$

to fit the band structure obtained from the first-principles calculation. U and J_H are the on-site intra-orbital Hubbard repulsion and Hund's coupling, respectively. We use the nonrotationally invariant Hund's coupling and have the interorbital Coulomb interaction $U' = U - 2J_H$ according to symmetry [28]. $\Delta_{iju} = V\langle c_{i\uparrow} c_{j\downarrow}\rangle$ is the intraorbital spin-singlet s^{+-} pairing bond order parameter and V is the next-nearest-neighbor intraorbital attraction.

In the presence of a magnetic field B perpendicular to the plane, the hopping integral is substituted by the Peierl's phase factor as

$$t_{ijuv} \to t_{ijuv} e^{i\frac{\pi}{\Phi_0}\int_{r_j}^{r_i} \mathbf{A}(r)\cdot dr},$$

where $\Phi_0 = hc/2e$ is the superconducting flux quantum, and $\mathbf{A} = (-By, 0, 0)$ is the vector potential in the Landau gauge. Here, we introduce the magnetic unit cell which accommodates two superconducting flux quanta. The linear dimension of the rectangular lattice is $N_x \times N_y$ where $N_x = 2N_y$. The size is larger than the coherence length ξ of the iron-pnictides [2].

The Hamiltonian (1) can be solved self-consistently through the Bogoliubov-de Gennes' equations,

$$\sum_{jv} \begin{pmatrix} H_{ijuv\uparrow} & \Delta_{ijuv} \\ \Delta^*_{ijuv} & -H^*_{ijuv\downarrow} \end{pmatrix} \begin{pmatrix} u^n_{jv} \\ v^n_{jv} \end{pmatrix} = E_n \begin{pmatrix} u^n_{iu} \\ v^n_{iu} \end{pmatrix},$$

where

$$H_{ijuv\sigma} = t_{ijuv\sigma} + \{-\mu + U\langle n_{iu\bar{\sigma}}\rangle + U'\langle n_{iv\sigma}\rangle + (U' - J_H)\langle n_{iv\bar{\sigma}}\rangle\}\delta_{ij}$$

The self-consistent parameters for the electron density and the pairing order parameter are given as follows,

$$\langle n_{i\uparrow}\rangle = \sum_n^{2N} |\mathbf{u}^n_i|^2 f(E_n)$$

$$\langle n_{i\downarrow}\rangle = \sum_n^{2N} |\mathbf{v}^n_i|^2 f(1 - E_n)$$

$$\Delta_{ij} = \frac{V}{2} \sum_n^{2N} \mathbf{u}^n_i \mathbf{v}^{n*}_j \tanh\left(\frac{\beta E_n}{2}\right)$$

where $\mathbf{u}^n_{i\uparrow} = (u^n_i \quad -v^{n*}_i)$, $\mathbf{v}^n_{i\downarrow} = (v^n_i \quad u^{n*}_i)$, and $f(E_n)$ is the Fermi distribution function. We solve the set of BdG equations above self-consistently. Once the self-consistency is achieved, the electron filling $\langle n\rangle$ is calculated. Here $\langle n\rangle$ is half of the value of the doping concentration x, i.e., $\langle n\rangle = x/2$.

The local density of states (LDOS) proportional to the differential tunneling conductance as measured by STM is expressed as,

$$\rho_i(E) = -\frac{1}{M_x M_y} \sum_{nu} [|\mathbf{u}^n_{iu}|^2 f'(E_n - E) + |\mathbf{v}^n_{iu}|^2 f'(E_n + E)]$$

where M_x and M_y is the number of magnetic unit cells. The size of a magnetic unit cell is $M_x \times M_y = 40 \times 40$. Throughout the paper, the length and energy are measured in units of the Fe-Fe distance a and t_1, respectively. In the following, the on-site Coulomb interaction U, Hund's coupling J_H, and next-nearest-neighbor attraction are respectively taken as $U = 3.5$, $J_H = 0.4$, and $V = 1.3$ to ensure that a vortex core can be completely enclosed inside a square lattice. We would study on different doping concentrations $x = 2.05$, 2.1, and 2.2, corresponding to the stripe SDW, nematic and SC states, respectively, in the presence of a magnetic field.

III. VORTEX CORES

For $x = 2.05$, we perform the vortex core in the stripe SDW state corresponding to the underdoped region. Figures 1(a) shows the spatial configurations of the s^{+-} wave superconductivity Δ_i. The superconductivity is vanished at the vortex center and starts to increase anisotropically along both x- and y-directions at the scale of the coherence length ξ to its bulk value. Figures 1(b) show the spatial configurations of the magnetization M_i. The magnetization shows the spins parallel along the y-axis and antiparallel along the x-axis, i.e., the modulation along the x-axis with wavelength $\lambda = 2a$ corresponding to the wavevector $Q_x = (\pi, 0)$. Around the vortex core center, the field enhances the magnetization and causes a small bump. Figures 1(c) show the spatial configurations of the charge density n_i. The charge density displays a depletion with an elliptic shape around the vortex core center.

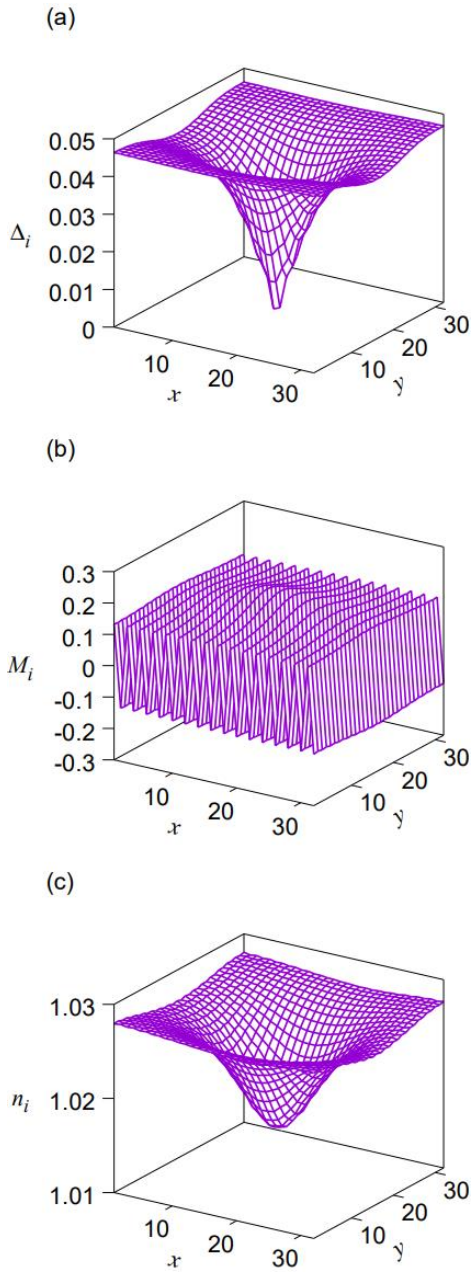

FIG. 1. (Color online) The spatial configurations of (a) the s^{+-} wave superconductivity Δ_i, (b) the magnetization M_i, and (c) the charge density n_i on a 32×32 lattice. The electron filling is $x = 2.05$ corresponding to the stripe SDW state.

For $x = 2.1$, we perform the vortex core in the nematic state corresponding to the optimally doped region. The superconductivity in Fig. 2(a) is vanished at the vortex center and starts to increase at the scale of the coherence length ξ to its bulk value, but the increase is gentle along the y-direction. The anisotropic coherence lengths make the vortex cores an oval shape. Furthermore, the magnetization in Fig. 2(b) can be described as

$$M_i = M_1 \cos(q_y \cdot r_i)\, e^{iQ_x \cdot r_i} + M_2 \sin(q_x \cdot r_i)\, e^{iQ_y \cdot r_i}$$

where the wavevectors $q_x = (2\pi/\lambda, 0)$ and $q_y = (0, 2\pi/\lambda)$ correspond to a modulation along the x-axis and the y-axis with wavelength $\lambda = 28a$. $Q_x = (\pi, 0)$ corresponds to the spins parallel along the y-axis and antiparallel along the x-axis. $Q_y = (0, \pi)$ corresponds to the spins parallel along the x-axis and antiparallel along the y-axis. $M_1 = 0.04$ and $M_2 = 0.06$ are the amplitude of the modulation of the bulk value [26]. In the presence of a magnetic field, the magnetization is slightly enhanced at the vortex core center which remains $M_1 \neq M_2$ and preserves the C_2 symmetry of a single vortex core. On the other hand, the charge density is depleted at the vortex core which is compensated by an enhancement of electrons around the vortex core. In addition, the charge density in Fig. 2(c) exhibits a modulation with period $14a$ and an oval shape of the vortex core.

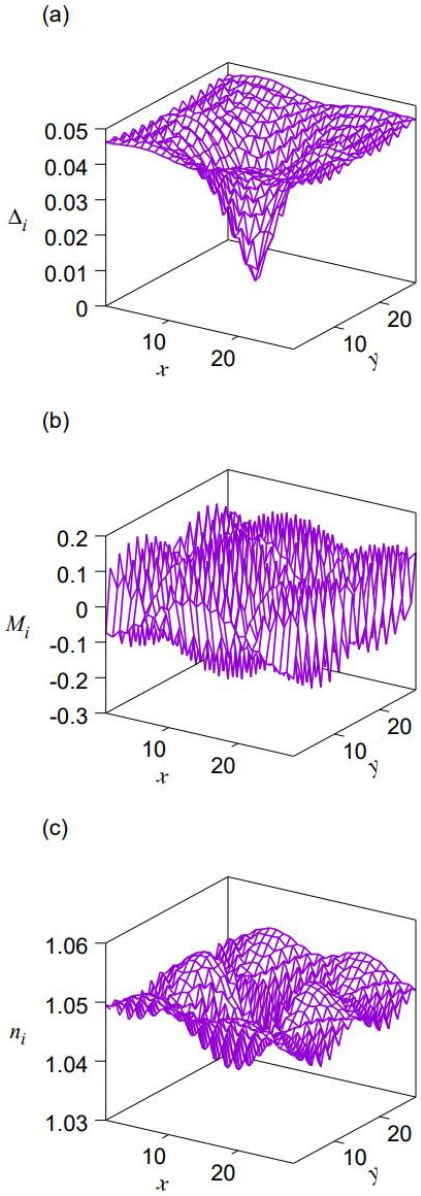

FIG. 2. (Color online) The spatial configurations of (a) the s^{+-} wave superconductivity Δ_i, (b) the magnetization M_i, and (c) the charge density n_i on a 28×28 lattice. The electron filling is $x = 2.1$ corresponding to the nematic state.

For $x = 2.2$, we perform the vortex core in the superconducting state corresponding to the overdoped region. Fig. 3(a) shows that the superconductivity goes to zero at the vortex core center and isotropically increases to its bulk values. The isotropic coherence lengths reveal a circular shape of the vortex core. Fig. 3(b) shows that the magnetization is fully suppressed inside the vortex core and outside the vortex core. Fig. 3(c) shows that the charge density is enhanced in the vortex core.

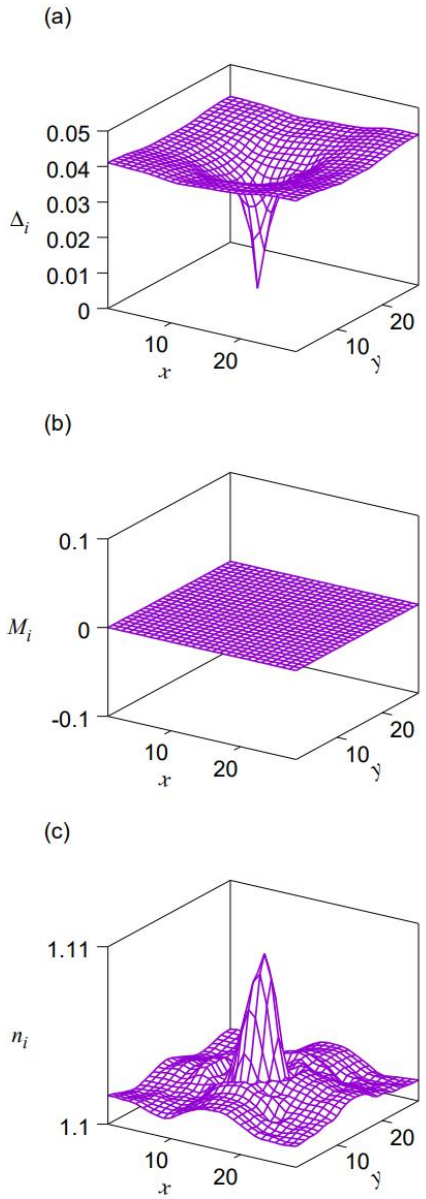

FIG. 3. (Color online) The spatial configurations of (a) the s^{+-} wave superconductivity Δ_i, (b) the magnetization M_i, and (c) the charge density n_i on a 28×28 lattice. The electron filling is $x = 2.2$ corresponding to the SC state.

IV. LOCAL DENSITY OF STATES

In order to further examine the differences among the vortex cores in the stripe SDW state, nematic state, and SC state, we perform the calculations of the LDOS at three electron dopings, i.e., $x = 2.05$, $x = 2.1$, and $x = 2.2$.

We examine the LDOS maps, which are the LDOS with fixed energy at each site of the magnetic unit cell, at various energies. In Fig. 4, the LDOS maps have been presented at energies ranging from 0.0 to 0.1 with $\Delta E = 0.02$ increments. Usually, the STM images obtained experimentally are results of integrating the spectral density between energies E_1 and E_2, which is defined as

$$S_i(E_1, E_2) = \sum_{E_1}^{E_2} \rho_i(E)\Delta E$$

There E_1 is taken to be 0 and E_2 has been set near the energy of the vortex core state.

The integrated spectrum $S_i(E_1, E_2)$ of the LDOS maps for $x = 2.05$ is shown in Fig. 4(a). It shows that the intensities of the elliptic bump are predominantly concentrated near the vortex core and decays rapidly away from the vortex core center. For $x = 2.1$ (as shown in Fig. 4(b)), the LDOS map shows that the intensities along the x-axis decay more rapidly than the one along the y-axis. The anisotropic distribution of the intensities of the integrated spectrum resulting in an oval shape of the vortex core, which are predominantly concentrated inside the vortex core. For $x = 2.2$ (as shown in Fig. 4(c)) the LDOS maps presents a circular bump around the vortex core center.

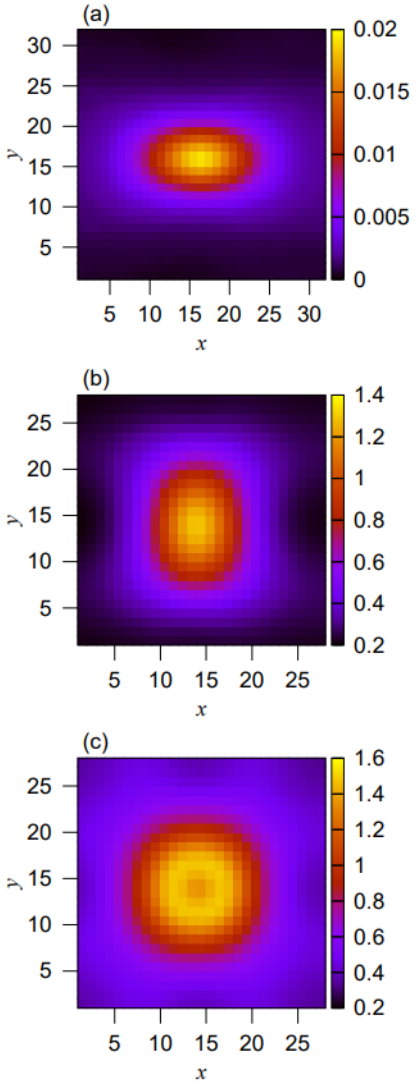

FIG. 4. (Color online) The spatial variation of the local density of states (LDOS maps) (a) $x = 2.05$ (b) $x = 2.1$ (c) $x = 2.2$. The integrated spectrum of $S_i(E_1, E_2)$ are from the Fermi energy to the upper bound of the vortex core state.

The LDOS as a function of energy have been presented at the vortex core center and at the site outside the vortex core given in Fig. 5(a), 5(b), and 5(c).

For $x = 2.05$, the existence of the stripe SDW order develops an SDW gap which shifts toward the negative energy of the LDOS (purple line in Fig. 5(a)). At the site outside the vortex core, the shifted SDW gap suppresses the intensities of superconducting coherence peak at the negative energy resulting in the prominently asymmetric coherence peaks (green line in Fig. 5(a)). At the vortex core center, the magnetization is slightly enhanced and the maximum value of the magnetization reaches $M_{\max} \simeq 0.21$. Meanwhile, the charge density depletes and results in a local hole-rich region. Nevertheless, the local SDW order push away the zero-bias resonance peak toward the positive energy as the behavior similar to the hole-doped iron-pnictide superconductors, such as $Ba_{1-x}K_xFe_2As_2$ [5].

For $x = 2.1$, figure 5(b) shows the LDOS in the nematic state. In the nematic state, the magnetization does not cause any SDW gap [25, 26]. Therefore, the LDOS at the site outside the vortex core exhibits only one kind of gap, i.e., the superconducting gap. At the vortex core center, the magnetization is slightly enhanced and the maximum value of the magnetization is $M_{\max} \simeq 0.16$. The developed local SDW order further splits the zero bias resonant peak. In addition, the states associated with these two peaks have been referred to as the vortex core states.

For $x = 2.2$, figure 5(c) shows a the sharp in-gap peak at the negative energy indicates the existence of the Andreev bound states as well. As the energy far away from the Fermi energy, the LDOS reach its bulk values. At the site outside the vortex core, the LDOS reveals two extra coherence peaks on the edges of the SC gap, which is a hallmark of two SC gaps (green line in Fig. 5(c)).

The LDOS maps shows that both the nematic state and the stripe SDW state exhibit elliptic shape. Nevertheless, the LDOS spectrum for the nematic state displays two-peak structure and the LDOS spectrum for the stripe SDW state shows one peak. This splitting of the LDOS at the vortex core center had been reported by the STM experiments on the optimally doped $BaFe_{1.8}Co_{0.2}As_2$ [2] can be explained with the existence of the nematic order. However, the elliptic shape of the vortex core still lack explicitly data to be verified.

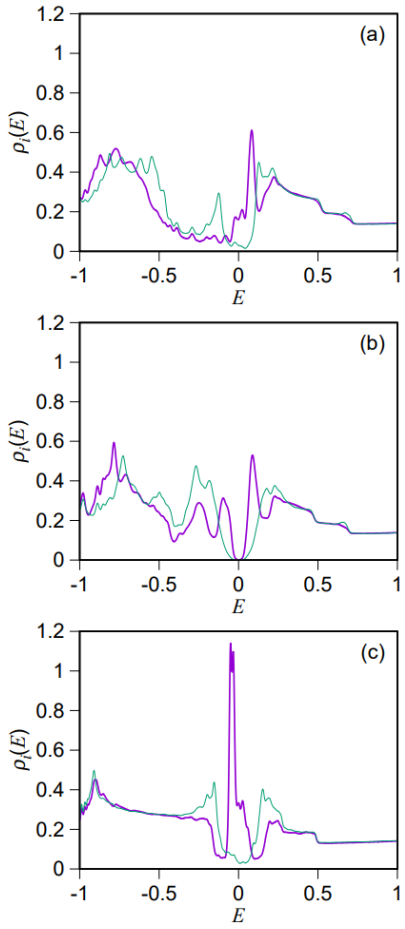

FIG. 5. (Color online) The local density of states at the vortex core center (purple line) and of the bulk values (green line) for (a) $x = 2.05$ (b) $x = 2.1$ (c) $x = 2.2$, respectively.

V. CONCLUSION

In conclusion, we have studied the vortex core among the nematic, stripe SDW, and SC states in electron-doped iron-pnictide superconductors such as $Ba(Fe_{1-x}Co_xAs)_2$ by using a two-orbital tight-binding model plus the magnetic interactions.

In the stripe SDW state, the LDOS maps exhibits an oval vortex core similar to the nematic state. Nevertheless, the stripe SDW order make as SDW gap which shifts toward the negative energy of the LDOS and suppresses one of the superconducting coherence peaks. At the vortex core center, the zero-bias resonance peak is pushed away toward the positive energy due to the induced magnetization inside the vortex core.

In the nematic state, the integrated spectrum of LDOS maps shows an oval shape of the vortex core. The magnetization is slightly enhanced inside the vortex core, and causes a significant splitting of the zero-bias resonance within the superconducting coherence gap. The LDOS displays distinct two peaks which are referred to the vortex core states and consistent with the STS experiments [2]. Outside the vortex core, even the existing of the magnetization, there are still no SDW gap.

In the SC state, the LDOS maps exhibits a circular vortex core. There is no SDW orders existing inside or outside of the vortex core. The LDOS shows a the sharp in-gap peak at the negative energy at the vortex core center. Outside the vortex core, the LDOS shows two extra peaks at the inner edge of the coherence peaks which provides the evidence of two SC gaps.

ACKNOWLEDGEMENTS

The author would thank C. C. Yang for useful discussions. The author is grateful to MoST of Taiwan (107-2112-M-003-002-) for supporting this study.

*Author to whom all correspondence should be addressed: hongyi@ntnu.edu.tw

[1] Lei Shan, Yong-Lei Wang, Bing Shen, Bin Zeng, Yan Huang, Ang Li, Da Wang, Huan Yang, Cong Ren, Qiang-Hua Wang, Shuheng H. Pan, Hai-Hu Wen, Nature Phys. 7, 325 (2011). https://doi.org/10.1038/nphys1908.

[2] Yi Yin, M. Zech, T. L. Williams, X. F. Wang, G. Wu, X. H. Chen, and J. E. Hoffman, Phys. Rev. Lett. 102, 097002 (2009). https://doi.org/10.1103/PhysRevLett.102.097002.

[3] Xiang Hu, C. S. Ting, and Jian-Xin Zhu, Phys. Rev. B 80, 014523 (2009). https://doi.org/10.1103/PhysRevB.80.014523.

[4] Tao Zhou, Z. D. Wang, Yi Gao, and C. S. Ting, Phys. Rev. B 84, 174524 (2011). https://doi.org/10.1103/PhysRevB.84.174524.

[5] Yi Gao, Huai-Xiang Huang, Chun Chen, C.S. Ting, and Wu-Pei Su, Phys. Rev. Lett. 106, 027004 (2011). https://doi.org/10.1103/PhysRevLett.106.027004.

[6] Xiang Hu, C. S. Ting, and Jian-Xin Zhu, Phys. Rev. B 80, 014523 (2009). https://doi.org/10.1103/PhysRevB.80.014523.

[7] Hong-Min Jiang, Jian-Xin Li, and Z. D. Wang, Phys. Rev. B 80, 134505 (2009). https://doi.org/10.1103/PhysRevB.80.134505.

[8] M. A. N. Araújo, M. Cardoso, and P. D. Sacramento, New J. Phys. 11, 113008 (2009). https://doi.org/10.1088/1367-2630/11/11/113008.

[9] Da Wang, Jian Xu, Yuan-Yuan Xiang, and Qiang-Hua Wang, Phys. Rev. B 82, 184519 (2010). https://doi.org/10.1103/PhysRevB.82.184519.

[10] J. Zhao, D. T. Adroja, D. X. Yao, R. Bewley, S. L. Li, X. F. Wang, G. Wu, X. H. Chen, J. P. Hu, and P. C. Dai, Nature Phys. 5, 555 (2009). https://doi.org/10.1038/nphys1336.

[11] Ming Yi, Donghui Lu, Jiun-Haw Chu, James G. Analytis, Adam P. Sorini, Alexander F. Kemper, Brian Moritz, Sung-Kwan Mo, Rob G. Moore, Makoto Hashimoto, Wei-Sheng Lee, Zahid Hussain, Thomas P. Devereaux, Ian R. Fisher, and Zhi-Xun Shen, PNAS 108, 6878 (2011). https://doi.org/10.1073/pnas.1015572108.

[12] T.-M. Chuang, M. P. Allan, Jinho Lee, Yang Xie, Ni Ni, S. L. Bud'ko, G. S. Boebinger, P. C. Canfield, and J. C. Davis, Science 327, 181 (2010). https://doi.org/10.1126/science.1181083.

[13] Jiun-Haw Chu, James G. Analytis, Kristiaan De Greve, Peter L. McMahon, Zahirul Islam, Yoshihisa Yamamoto, and Ian R. Fisher, Science 329, 824 (2010). https"//doi.org/10.1126/science.1190482.

[14] Jiun-Haw Chu, James G. Analytis, David Press, Kristiaan De Greve, Thaddeus D. Ladd, Yoshihisa Yamamoto, and Ian R. Fisher, Phys. Rev. B 81, 214502 (2010). https://doi.org/10.1103/PhysRevB.81.214502.

[15] T. Shimojima, K. Ishizaka, Y. Ishida, N. Katayama, K. Ohgushi, T. Kiss, M. Okawa, T. Togashi, X.-Y. Wang, C.-T. Chen, S. Watanabe, R. Kadota, T. Oguchi, A. Chainani, and S. Shin, Phys. Rev. Lett. 104, 057002 (2010). https://doi.org/10.1103/PhysRevLett.104.057002.

[16] M. A. Tanatar, E. C. Blomberg, A. Kreyssig, M. G. Kim, N. Ni, A. Thaler, S. L. Bud'ko, P. C. Canfield, A. I. Goldman, I. I. Mazin, and R. Prozorov, Phys. Rev. B 81, 184508 (2010). https://doi.org/10.1103/PhysRevB.81.184508.

[17] L. W. Harriger, H. Q. Luo, M. S. Liu, C. Frost, J. P. Hu, M. R. Norman, and Pengcheng Dai, Phys. Rev. B 84, 054544 (2011). https://doi.org/10.1103/PhysRevB.84.054544.

[18] M. Nakajima, T. Liang, S. Ishida, Y. Tomioka, K. Kihou, C. H. Lee, A. Iyo, H. Eisaki, T. Kakeshita, T. Ito, and S. Uchida, PNAS 108, 12238 (2011). https://doi.org/10.1073/pnas.1100102108.

[19] Hsueh-Hui Kuo, Jiun-Haw Chu, Scott C. Riggs, Leo Yu, Peter L. McMahon, Kristiaan De Greve, Yoshihisa Yamamoto, James G. Analytis, and Ian R. Fisher, Phys. Rev. B 84, 054540 (2011). https://doi.org/10.1103/PhysRevB.84.054540.

[20] S. Kasahara, H. J. Shi, K. Hashimoto, S. Tonegawa, Y. Mizukami, T. Shibauchi, K. Sugimoto, T. Fukuda, T. Terashima, Andriy H. Nevidomskyy, and Y. Matsuda, Nature 486, 382 (2012). https://doi.org/10.1038/nature11178.

[21] Jiun-Haw Chu, Hsueh-Hui Kuo, James G. Analytis, and Ian R. Fisher, Science 337, 710 (2012). https://doi.org/10.1126/science.1221713.

[22] Rafael M. Fernandes, Anna E. Böhmer, Christoph Meingast, and Jörg Schmalian, Phys. Rev. Lett. 111, 137001 (2013). https://doi.org/10.1103/PhysRevLett.111.137001.

[23] E. C. Blomberg, M. A. Tanatar, R. F. Fernandes, I. I. Mazin, B. Shen, H.-H. Wen, M. D. Johannes, J. Schmalian, and R. Prozorov, Nature Comm. 4, 1914 (2013). https://doi.org/10.1038/ncomms2933.

[24] C. Mirri, A. Dusza, S. Bastelberger, J.-H. Chu, H.-H. Kuo, I. R. Fisher, and L. Degiorgi, Phys. Rev. B 90, 155125 (2014). https://doi.org/10.1103/PhysRevB.90.155125.

[25] Morten H. Christensen, Jian Kang, Brian M. Andersen, and Rafael M. Fernandes, Phys. Rev. B 93, 085136 (2016). https://doi.org/10.1103/PhysRevB.93.085136.

[26] Chung-Pin Chou, Hong-Yi Chen, C. S. Ting, Physica C 546, 61 (2018). https://doi.org/10.1016/j.physc.2017.12.009.

[27] Y. Y. Tai, J.-X. Zhu, J. G. Matthias, and C. S. Ting, EPL 103, 67001 (2013). https://doi.org/10.1209/0295-5075/103/67001.

[28] P. Ghaemi, F. Wang, and A. Vishwanath, Phys. Rev. Lett. 102, 157002 (2009). https://doi.org/10.1103/PhysRevLett.102.157002.